Electrochimica Acta 71 (2012) 50–57

Contents lists available at SciVerse ScienceDirect

Electrochimica Acta

journal homepage: www.elsevier.com/locate/electacta

The role of Ni in the surface stability of Cu–Al–Ni ternary alloys in sulfate–chloride solutions

W.A. Badawy[a,*], M. El-Rabiee[b], N.H. Helal[b], H. Nady[b]

[a] Chemistry Department, Faculty of Science, Cairo University, 12 613 Giza, Egypt
[b] Chemistry Department, Faculty of Science, Fayoum University, Fayoum, Egypt

ARTICLE INFO

Article history:
Received 25 January 2012
Received in revised form 14 March 2012
Accepted 15 March 2012
Available online 4 April 2012

Keywords:
Chloride ions
Cu–Al–Ni alloys
Cyclic voltammetry
Impedance
Passive films

ABSTRACT

The stability of Cu–Al–Ni ternary alloys used in the manufacturing of NaCl and Na_2SO_4 from Lake Qaroun in Egypt was investigated in sulfate–chloride electrolytes. Different electrochemical techniques were used. The results show that the increase in the nickel content improves the stability of the ternary alloys due to formation of a stable barrier film. The barrier film behaves like an ideal capacitor and its stability is affected by the chloride ion concentration. An equivalent circuit model for the electrode/electrolyte interface was proposed and the experimental impedance data were fitted to theoretical data according to this model. The surface morphology and barrier layer constituents were investigated by SEM/EDAX unit.

1. Introduction

Due to high thermal conductivity, good resistance to corrosion and good mechanical workability, copper and copper alloys are widely used as condenser and heat exchanger tubing materials in power plants, and other industries. These materials are preferred in sea water applications because of the resistance to bio-fouling resulting from the action of a low level steady discharge of Cu (II) ions. The alloys have received widespread applications as a welded cladding for steel offshore structures and ship hulls [1]. The corrosion behavior of the material depends heavily on the nature of the barrier film formed on its surface. The structure of this film was found to consist of two layers, an outer CuO layer with chemisorbed water molecules and traces of chloride ions, and an inner Cu_2O layer containing Ni^{2+} and Ni^{3+} [2]. The presence of aluminum increases the corrosion resistance of the alloy, especially in neutral solutions and seawater; it provides good wear properties and resistance to high temperature oxidations [3,4]. The good corrosion resistance of the Cu–Al–Ni alloys in neutral solutions is due to the presence of a protective layer of alumina, which builds up quickly on the surface post-exposure to the corrosive environment and the passivation process is based on the fact that aluminum has a greater affinity towards oxygen than copper and considerable stability of Al_2O_3 than Cu_2O in neutral solutions [5–7]. The essential role of Ni in the passivation of Cu–Ni alloys has been attributed to its incorporation into the Cu (I) oxide which is formed as corrosion product [8]. The incorporation of nickel ions reduces the number of cation vacancies that normally exist in Cu (I) oxide [9]. The tremendous application of copper/nickel alloys in different industries, where chloride containing water is always used, make the understanding of the electrochemical behavior of these alloys in the presence of chloride ions and the control of the corrosion process important subjects worthy of intensive investigations. In one of our previous investigations we have recommended the use of Cu–10Al–5Ni alloy in the production of Na_2SO_4 and NaCl from Lake Qaroun in Egypt [10]. In this paper we are aiming at the understanding of the role of Ni in the stability of the Cu–Al–Ni ternary alloys with constant Al ratio of 10% in neutral sulfate–chloride solutions.

2. Experimental details

The working electrodes were made from commercial grade Cu–Al–Ni rods, mounted into glass tubes by two-component epoxy resin leaving a surface area of 0.2 cm^2 to contact the solution. The alloys were prepared in our metallurgical institute and the mass spectrometric analysis of the electrodes used is presented in Table 1. The electrochemical cell was a three-electrode all-glass cell, with a platinum counter electrode and saturated calomel, SCE, reference electrode. Before each experiment, the working electrode

* Corresponding author. Tel.: +20 2 3567 6558; fax: +20 2 35685799.
E-mail addresses: wbadawy@cu.edu.eg, wbadawy50@hotmail.com (W.A. Badawy).

0013-4686/$ – see front matter © 2012 Elsevier Ltd. All rights reserved.
doi:10.1016/j.electacta.2012.03.053

Table 1
Mass spectrometric analysis for the different electrode materials in mass%.

Sample	Cu	Al	Ni	Zn	Mn	Sn	Fe	Si	Mg	Ti
Cu–Al–5Ni	81.16	11.15	4.98	0.11	0.02	0.14	2.22	0.21	0.01	–
Cu–Al–10Ni	76.00	11.28	9.95	0.10	0.02	0.14	2.26	0.24	0.01	–
Cu–Al–30Ni	60.02	9.32	29.17	0.08	0.01	0.13	1.10	0.16	0.01	–
Cu–Al–45Ni	43.31	9.56	46.01	–	–	0.04	0.72	0.35	–	0.01

was polished mechanically using successive grades emery papers down to 2000 grit. The electrode was washed thoroughly with distilled water, and transferred quickly to the cell. The electrochemical measurements were carried out in a stagnant, naturally aerated sulfate–chloride solution (0.5 M Na_2SO_4 + 0.5 M NaCl) and the pH of the solution was adjusted to 7 by drops of H_2SO_4 or NaOH.

The polarization experiments and electrochemical impedance spectroscopic investigations, EIS, were performed using a Voltalab PGZ 100 "All-in-one" potentiostat/galvanostat. The potentials were measured against and referred to the standard potential of the SCE (0.245 V vs. the standard hydrogen electrode, SHE). The polarization experiments were carried out using a scan rate of 1 mV s^{-1}, and the cyclic voltammetry measurements were carried out using a scan rate of 10 mV s^{-1}. The scan rate was selected after measurements in the range 2–250 mV s^{-1} to avoid large electrochemical and chemical dissolution process at $\upsilon < 5$ mV s^{-1} or loss in the definition of different oxidation process at $\upsilon > 50$ mV s^{-1} [11]. The potential range was chosen to record any cathodic step that could be present before any anodic dissolution. The total impedance, Z, and phase shift, θ, were recorded in the frequency domain 0.1–10^5 Hz. The superimposed ac-signal was 10 mV peak to peak amplitude. The surface morphology and the constituent elements of the passive film were investigated by SEM/EDAX (model ISPECT S 2006, FEI Company, Holland). Each experiment was carried out at least twice and details of experimental procedures are as described elsewhere [10,12].

3. Results and discussion

The open-circuit potentials of Cu, Ni and Cu–Al–Ni alloys with different Ni contents (5, 10, 30 and 45 mass% Ni) were traced over 60 min in the test solution. Unlike the behavior of the alloys in chloride free neutral solutions, the open circuit potential of alloys with Ni content < 30% shift towards negative values and lie in the range of pure Cu. Alloys with 45% Ni show less negative open circuit potential values and lie in the range of pure nickel [13]. The steady-state potential was, generally reached within 15 min from electrode immersion in the electrolyte and was found to be affected by chloride ions. The increase of chloride ion concentration shifts the steady state potential towards more negative values.

3.1. Cyclic voltammetric investigations

The cyclic voltammograms of the alloys under investigation and also those of Cu, Ni, were recorded in a stagnant, naturally aerated neutral 0.5 M Na_2SO_4 + 0.5 M NaCl solution at a scan rate of 10 mV s^{-1} and 25 °C. Typical cyclic voltammogram for Ni is shown in Fig. 1a. The scan was initiated at −0.8 V where a transition region, before the active metal dissolution, was recorded. This region is due to the formation of adsorbed species such as $Ni(H_2O)_{ads}$ and/or $NiClOH^-{}_{ads}$ at the electrode surface via the following reactions [14,15].

$$Ni + H_2O \rightarrow Ni(H_2O)_{ads} \quad (1)$$

$$Ni + H_2O + Cl^- \rightarrow NiClOH_{ads}{}^- + H^+ + e^- \quad (2)$$

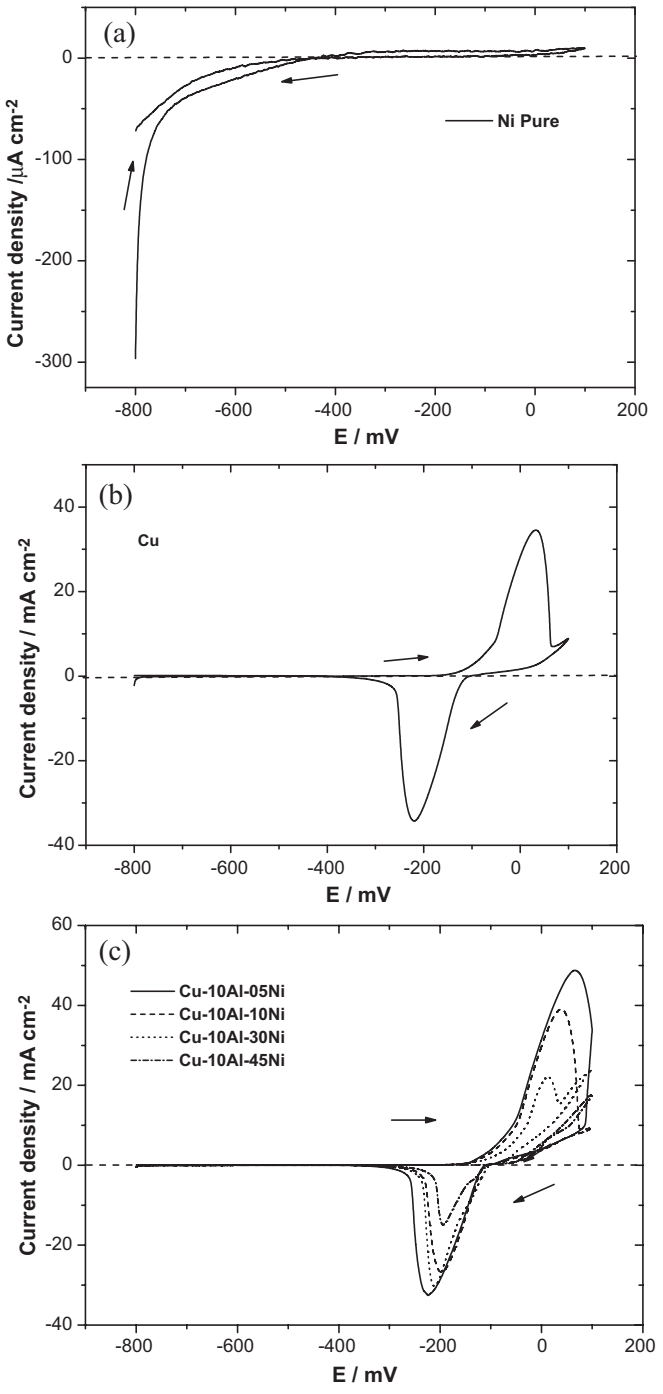

Fig. 1. Cyclic voltammograms of Ni (a), Cu (b) and Cu–Al–Ni alloys (c) in a stagnant naturally aerated 0.5 M $SO_4{}^{-2}$ + 0.5 M Cl^- solution of pH 7.0 at 25 °C and scan rate of 10 mVs^{-1}.

In the active region, the anodic current density increases with increasing the anodic potential due to the dissolution of the adsorbed species according to the following reactions:

$$Ni(H_2O)_{ads} + 2Cl^- \rightarrow NiCl_2 + H_2O + 2e^- \quad (3)$$

$$NiClOH_{ads}{}^- + Cl^- \rightarrow NiCl_2 + OH^- + e^- \quad (4)$$

The dissolution of the intermediate species produces new active sites on the electrode surface, and the formation of the passive film is hindered leading to localized corrosion [16].

Fig. 1b presents typical cyclic voltammogram for Cu in the same solution and under the same conditions. Also, a transition region before the active metal dissolution, in which the current density stabilizes with potential was recorded. This transition region is due to the formation of intermediate species on the electrode surface [17,18] via reactions, such as:

$$Cu + H_2O \rightarrow CuH_2O_{ads} \quad (5)$$

$$Cu + OH^- \rightarrow CuOH_{ads}{}^- \quad (6)$$

$$Cu + Cl^- \rightarrow CuCl_{ads}{}^- \quad (7)$$

The solubility of $CuCl_{ads}{}^-$ is low, so it precipitates on the electrode surface forming a porous CuCl film [19].

In the anodic region, the current density increases rapidly with increasing potential due to the formation of the soluble $CuCl_2{}^-$ and formation of other soluble species according to [20]:

$$Cu + 2Cl^- \rightarrow CuCl_2{}^- + e^- \quad (8)$$

$$CuCl + Cl^- \rightarrow CuCl_2{}^- \quad (9)$$

also

$$CuOH_{ads}{}^- + OH^- \rightarrow Cu(OH)_{2\,aq}{}^- + e^- \quad (10)$$

At higher chloride concentration ($[Cl^-] > 1.0\,mol\,dm^{-3}$), Cu complexes such as $CuCl_3{}^{2-}$ and $CuCl_4{}^{3-}$ can be formed [21]. It was suggested that the presence of high concentration of $CuCl_2{}^-$ at the metal surface leads to hydrolysis reaction and the formation of Cu_2O [22].

$$2CuCl_2{}^- + H_2O \rightarrow Cu_2O + 4Cl^- + 2H^+ \quad (11)$$

The formation of Cu_2O layer explains the decrease of the anodic current density. In the reverse scan, a clear cathodic peak appears at ~ −0.25 V due to the reduction of copper ions.

The cyclic voltammograms of the Cu–Al–5Ni, Cu–Al–10Ni, Cu–Al–30Ni and Cu–Al–45Ni alloys recorded under the same conditions are presented in Fig. 1c. The shapes of the cyclic voltammograms of the alloys resemble that of pure Cu more than that of

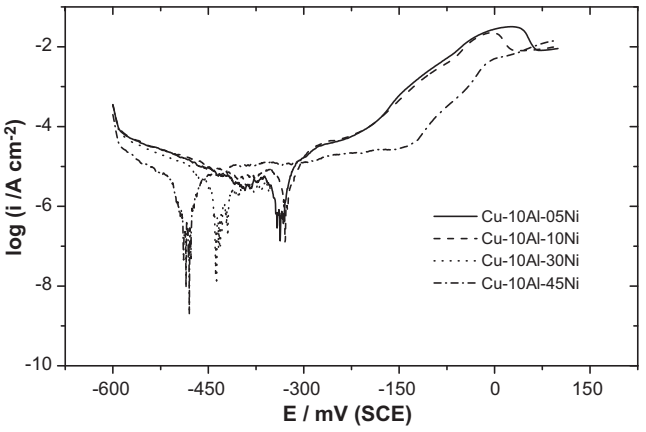

Fig. 2. Potentiodynamic polarization curves for the Cu–Al–Ni alloys in 0.5 M $SO_4{}^{-2}$ + 0.5 M Cl^- solution of pH 7 at 25 °C and scan rate of 5 mVs^{-1}.

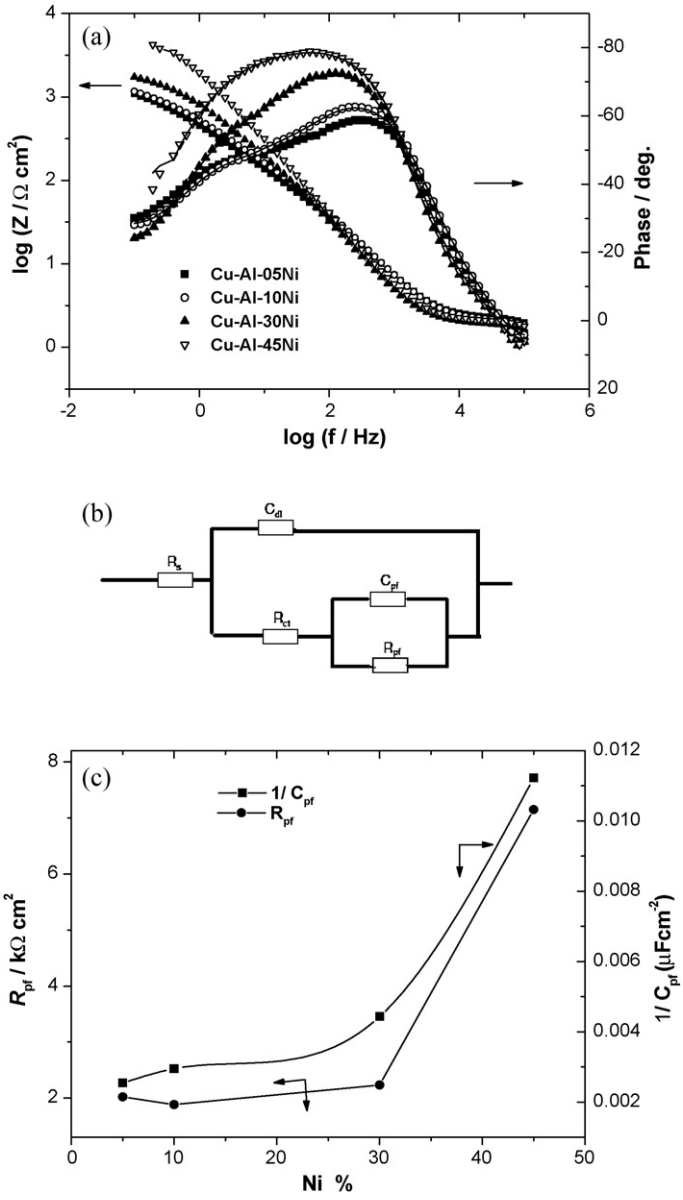

Fig. 3. (a) Bode plots of the Cu–Al–Ni alloys after 3 h immersion in a stagnant naturally aerated 0.5 M $SO_4{}^{-2}$ + 0.5 M Cl^- neutral solution at 25 °C. (b) Equivalent circuit model used in the impedance data fitting. Where R_s = solution resistance, R_p = charge-transfer resistance, C_{dl} = double layer capacitance, R_{pf} = passive film resistance, and C_{pf} = passive film capacitance. (c) The barrier film resistance, R_{pf}, and relative film thickness, $1/C_{pf}$, formed on the alloy surface in stagnant naturally aerated 0.5 M $SO_4{}^{-2}$ + 0.5 M Cl^- neutral solution at 25 °C, as a function of the Ni content.

Ni and the values of the anodic and cathodic peak current decreases with the increase in the Ni content.

3.2. Potentiodynamic polarizations

The potentiodynamic polarization curves of the Cu–Al–Ni alloys under investigation are presented in Fig. 2. The corrosion current density, i_{corr}, and corrosion potential, E_{corr}, were calculated using the potentiodynamic polarization data and presented in Table 2. It is worthwhile to mention that the recorded corrosion potentials are more positive than the open circuit-potential. A difference of about 200 mV was recorded which was attributed to a prepassivation step [23]. The corrosion current density measured after 1 h of electrode immersion in the solution decreases as the Ni content increases

Table 2
Potentiodynamic polarization parameters of Cu–10Al–XNi alloys after 1 h of electrode immersion, in 0.5 M SO_4^{-2} + 0.5 M Cl^- solution pH 7.0.

Alloys	E_{corr}/mV	i_{corr}/μA/cm²	β_a/mV	β_c/mV	Corrosion rate/mm Y^{-1}
Cu–Al–05Ni	−337.3	3.1	59.2	−181.9	36.8
Cu–Al–10Ni	−327.0	2.6	46.8	−26.8	30.1
Cu–Al–30Ni	−435.0	2.0	21.6	−63.7	23.9
Cu–Al–45Ni	−497.1	1.5	82.2	−63.4	17.9

due to the incorporation of Ni ions in the mobile vacancies of the Cu_2O film. The simultaneous dissolution of the alloy leads to the formation of monovalent Cu^+ which undergoes further oxidation to the more stable Cu^{2+} ion [24].

Generally, the corrosion behavior of the Cu–Al–Ni alloys is based on the common system of oxidation resistant materials, where Al has greater affinity towards oxygen than Cu. Under standard conditions, Al_2O_3 is almost eleven times more stable than Cu_2O relative to their metals in the zero oxidation state [6]. For Cu–10%Al alloys, thermal oxidation is based on a rapid initial production of Cu_2O then formation of Al_2O_3 at the alloy/oxide interface due to the depletion of Cu [25]. In neutral solutions, alumina forms as a protective oxide which is highly impermeable to the passage of Cu (I) ions which can no longer enter the outermost layer. The higher the aluminum content of the alloy, the greater the corrosion resistance due to the protective Al_2O_3 film since the limiting mole fraction is

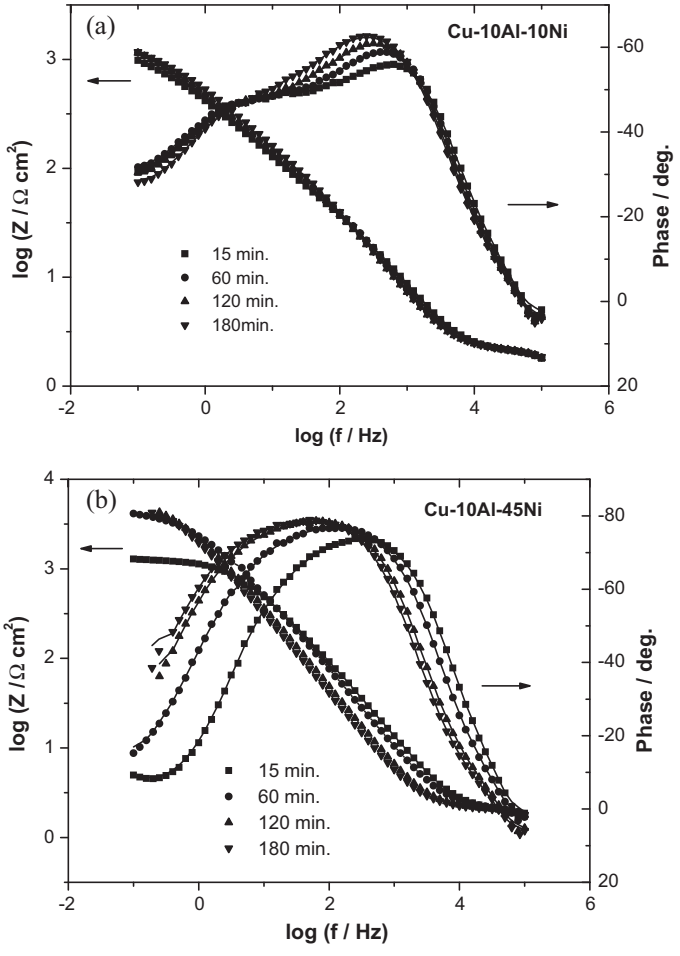

Fig. 4. (a) Bode plots of Cu–10Al–10Ni alloys after different times of immersion in stagnant naturally aerated 0.5 M SO_4^{-2} + 0.5 M Cl^- neutral solution at 25 °C. (b) Bode plots of Cu–10Al–45Ni alloys after different times of immersion in stagnant naturally aerated 0.5 M SO_4^{-2} + 0.5 M Cl^- neutral solution at 25 °C.

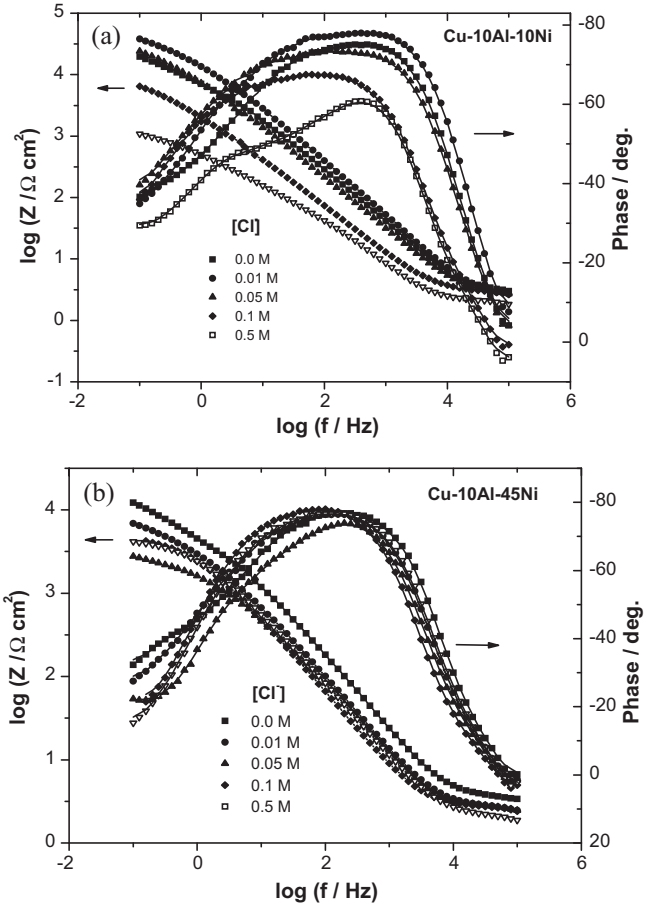

Fig. 5. (a) Bode plots of Cu–10Al–10Ni alloy after 1 h of immersion in 0.5 M SO_4^{-2} neutral solutions containing different chloride ion concentrations at 25 °C. (b) Bode plots of Cu–10Al–45Ni alloy after 1 h of immersion in 0.5 M SO_4^{-2} neutral solutions containing different chloride ion concentrations at 25 °C.

achieved over a shorter exposure time and is maintained at lower copper dissolution rates [25]. Keeping the Al% constant and changing the ratio of Ni, enrichment of Ni to the metallic surface takes place.

From the polarization data, the values of the corrosion current density are generally decreased with increasing the nickel content which means that the composition of the barrier Cu_2O layer formed on Cu and Cu–Al–Ni alloys is not identical. Nickel ions are incorporated into the crystal lattice of Cu_2O, as already reported by several authors [26,27] and the number of cation vacancies decreases with increasing the nickel content [9]. Ni from the alloy segregates into the Cu_2O barrier layer via a solid state reaction and Ni^{2+} interact with mobile cation vacancies which leads to a decrease in the ionic conductivity and increase of the electronic conductivity of the barrier film and the corrosion resistance thus increased [28,29].

The understanding of the interaction between cation and anion vacancies can give a good explanation of the effect of chloride ion on the corrosion resistance of the Cu-based alloys. The chloride ions are capable of occupying the oxygen vacancies and the following reaction occurs:

$$V_O^{2-}(ox) + Cl^- nH_2O = Cl_O^-(ox) + nH_2O + 2e^- \quad (12)$$

where $V_O^{2-}(ox)$; is an oxygen vacancy and $Cl^- nH_2O$ is a solvated chloride ion in the aqueous electrolyte. An equivalent number of cation vacancies must form through dissolution of the cation in the electrolyte according to:

$$2\,Cu(ox) = 2\,Cu^+(aq) + V^{2-}(ox) \quad (13)$$

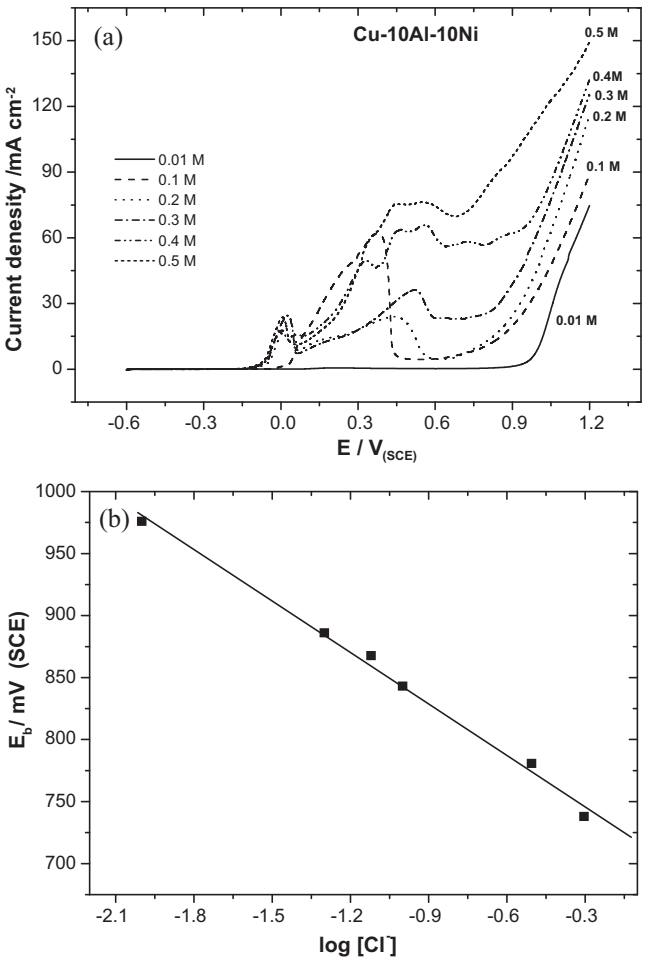

Fig. 6. (a) Anodic polarization of Cu–10Al–10Ni alloy in stagnant naturally aerated neutral solutions of 0.5 M SO_4^{-2} containing different concentrations of Cl^- at scan rate of 5 mVs^{-1} and 25 °C. (b) Effect of chloride ions on the breakdown potential of the Cu–10Al–10Ni alloy in neutral sulfate solution at 25 °C.

Therefore, the presence of chloride ions leads to an enhanced flux of cation vacancies from the oxide/electrolyte towards the metal/oxide interface. As the amount of incorporated chloride ions increases, the number of occupied oxygen vacancies increases and the film becomes unstable and localized breakdown occurs.

In the case of the barrier film formed on Cu–Al–Ni alloys in the presence of chloride ions, the process of nickel incorporation from the metal/oxide interface plays an important role. It seems reasonable to assume that a Cu_2O layer "doped" with nickel should exhibit a superior corrosion resistance compared to a "simple" Cu_2O layer [30].

3.3. Electrochemical impedance spectroscopic investigations

To confirm the polarization measurements, EIS investigations were carried out.

3.3.1. Effect of the Ni content

The impedance data of the different alloys recorded after 180 min of electrode immersion in the stagnant, naturally aerated neutral 0.5 M Na_2SO_4 + 0.5 M NaCl solutions are presented in Fig. 3a. The data were presented as Bode plots, since this format enables equal presentation of impedance data and the appearance of the phase angle as a sensitive parameter for any interfacial phenomena. The Bode plots of the alloys show two phase maxima, which indicate the presence of two time constants representing the electrode processes. These two phase maxima become closer and overlap as the Ni content increases. The impedance data were analyzed using software provided with the impedance system where the dispersion formula was used. For a simple equivalent circuit model consisting of a parallel combination of a capacitor, C_{dl}, and a resistor, R_p, in series with a resistor, R_s, representing the solution resistance, the electrode impedance, Z, is represented by the mathematical formulation:

$$Z = R_s + \left[\frac{R_p}{\{1 + (2\pi f R_p C_{dl})^{\alpha}\}}\right] \quad (14)$$

where α denotes an empirical parameter ($0 \le \alpha \le 1$) and f is the frequency in Hz [31,32]. To account for the presence of a passive film, the impedance data were analyzed using the equivalent circuit model shown in Fig. 3b where another combination R_{pf} C_{pf} representing the passive film resistance, R_{pf}, and the passive film capacitance, C_{pf}, was introduced. The calculated equivalent circuit parameters for the different alloys are presented in Table 3. The time constant at the intermediate frequencies is originated from the R_pC_{dl} combination while that at low frequencies is due to the $R_{pf}C_{pf}$ combination. The passive film resistance, R_{pf}, increases with the increase of the Ni content, which is in agreement with the polarization experiments. The passive film thickness which is directly proportional to $1/C_{pf}$, increases with the increase of Ni content [3]. The effect of the Ni content on the passive film resistance, R_{pf}, and the passive film thickness, $1/C_{pf}$, is presented in Fig. 3c.

3.3.2. Effect of alloy immersion time

The impedance data were recorded after different time intervals of electrode immersion in the test solution. The calculated values of the equivalent circuit parameters of these measurements are summarized in Table 4. It is worthwhile to mention that the alloys with Ni content ≥ 30% show two phase maxima corresponding to two time constants. Example of these results is the Bode plots of the Cu–10Al–10Ni presented in Fig. 4a. The phase angle and the overlap of the phase maxima change with the time of alloy immersion in the solution. The value of the phase angle especially that occurs at lower frequencies increases with the increase of the immersion time. This indicates a decrease in the corrosion rate which is reflected on the increase of the film resistance, R_{pf} (cf. Table 4). For higher Ni-content e.g. the Cu–Al–45Ni alloy, only one time constant is present, and the phase maximum broadens with the increase of the immersion time reaching the passive behavior (cf. Fig. 4b) [33].

3.3.3. Effect of chloride ion concentration

In this series of experiments the impedance behavior of the different alloys in a stagnant, naturally aerated neutral 0.5 M Na_2SO_4

Table 3
Equivalent circuit parameters for the different Cu–Al–Ni alloys after 3 h of alloy immersion in 0.5 M Na_2SO_4 + 0.5 M NaCl neutral solution at 25 °C.

Ni %	R_s/Ω	$R_{ct}/\Omega\,cm^2$	$C_{dl}/\mu F\,cm^{-2}$	α_1	$R_{pf}/k\Omega\,cm^2$	$C_{pf}/\mu F\,cm^{-2}$	α_2
5 Ni	1.95	218.3	18.2	0.99	2.02	394.0	1.0
10 Ni	1.93	251.8	15.8	0.99	1.88	339.0	1.0
30 Ni	1.80	537.4	14.8	0.99	2.23	225.7	0.99
45 Ni	2.03	2860	4.5	0.99	7.15	89.1	0.99

Table 4
Equivalent circuit parameters of the Cu–Al–Ni alloys in 0.5 M Na_2SO_4 + 0.5 M NaCl neutral solution recorded after different immersion times at 25 °C.

	Time/min	R_s/Ω	$R_{ct}/k\Omega\,cm^2$	$C_{dl}/\mu F\,cm^{-2}$	α_1	$R_{pf}/k\Omega\,cm^2$	$C_{pf}/\mu F\,cm^{-2}$	α_2
Cu–Al–5Ni	15	1.81	0.13	15.4	0.99	1.55	410.5	0.99
	60	1.97	0.21	18.82	0.99	1.86	428.6	0.99
	120	1.94	0.17	19.2	0.99	2.04	390.6	1.0
	180	1.95	0.22	18.2	0.99	2.02	394.0	1.0
Cu–Al–10Ni	15	1.87	0.12	13.4	0.99	1.66	383.6	0.99
	60	1.74	0.25	19.61	0.99	1.63	307.9	0.99
	120	1.92	0.21	15.5	0.99	2.16	369.2	1.0
	180	1.93	0.25	15.8	0.99	1.88	339.0	1.0
Cu–Al–30Ni	15	1.64	0.32	12.3	0.99	1.26	199.3	0.99
	60	1.59	0.34	18.60	0.99	1.63	308.1	0.99
	120	1.74	0.51	15.5	0.99	2.12	237.4	0.99
	180	1.80	0.54	14.8	0.99	2.23	225.7	0.99
Cu–Al–45Ni	15	1.89	0.75	2.7	1.0	1.29	38.91	0.99
	60	1.98	2.55	4.99	0.99	4.77	52.67	0.99
	120	1.99	3.03	4.2	1.0	6.46	98.53	0.99
	180	2.03	2.86	4.5	0.99	7.15	89.08	0.99

solution containing different NaCl concentrations was recorded. The impedance data were fitted to the theoretical data according to the equivalent circuit model of Fig. 3b and the calculated values are presented in Table 5. The presence of Cl^- ions decreases the passive film resistance for all alloys. Fig. 5a and b represents typical Bode plots recorded for Cu–10Al–10Ni and Cu–10Al–45Ni in the sulfate solution containing different Cl^- concentrations. It is important to mention that the calculated values of α_1 and α_2 in all solutions approaching unity which means that the electrode/electrolyte interface with its passive film behaves like an ideal capacitor [18].

The effect of chloride ion on the stability of the passive film can be understood by the investigation of the breakdown potential obtained from the anodic potentiodynamic polarization of the alloy in neutral sulfate solutions containing different concentration of Cl^-. Fig. 6a presents typical potentiodynamic polarization curves for Cu–10Al–10Ni. It is clear that the breakdown potential, E_b, decreases as the chloride ion concentration increases. The anodic polarization exhibits well defined anodic peaks corresponding to the alloy dissolution to Cu^+ then to Cu^{2+} [20] followed by a passive region and finally a sudden increase in the anodic current at the breakdown potential, E_b. The anodic peak current increases as the chloride ion concentration increases and at the same time E_b gets more negative. The breakdown potential, E_b, decreases linearly with log [Cl^-] as presented in Fig. 6b.

The surface morphology of the different alloys after 3 h immersion in stagnant naturally aerated neutral 0.5 M Na_2SO_4 + 0.5 M NaCl solution was investigated by SEM. Alloys with Ni content < 30% show clear corrosion patterns and flawed regions. Fig. 7a shows a typical SE micrograph of the Cu–10Al–10Ni alloy, where the corrosion sites are clearly observed. Alloys with 45% Ni did no show any flawed regions, which mean that the increase of the Ni content improves the stability of the alloy as was demonstrated by the polarization and impedance investigations (cf. Fig. 7b). The surface of the Cu–10Al–10Ni was subjected to EDAX analysis to record the different constituents of the barrier layer. Fig. 7c presents the result of this investigation. The method is not sensitive enough to show the very thin barrier film constitution. It shows mainly the constituent elements of the alloy itself. Generally, the three elements, Al, Cu, and Ni are participating in the passivation process and

Table 5
Equivalent circuit parameters of the Cu–Al–Ni alloys after 1 h. of electrode immersion in 0.5 M Na_2SO_4 solution containing different chloride ion concentrations at pH 7.0 at 25 °C.

	Cl^-/M	R_s/Ω	$R_{ct}/k\Omega\,cm^2$	$C_{dl}/\mu F\,cm^{-2}$	α_1	$R_{pf}/k\Omega\,cm^2$	$C_{pf}/\mu F\,cm^{-2}$	α_2
Cu–Al–5Ni	0.0	27.45	10.93	2.30	0.96	83.08	15.32	0.99
	0.01	11.67	18.98	2.65	0.99	67.12	14.98	1.0
	0.05	3.42	12.02	2.65	0.99	55.86	22.79	1.0
	0.1	1.85	1.03	30.76	0.99	3.13	254.0	0.99
	0.3	1.94	0.38	21.21	0.99	3.5	287	1.0
	0.5	1.97	0.21	18.82	0.99	1.86	428.6	0.99
Cu–Al–10Ni	0.0	2.16	7.27	1.75	0.99	49.2	16.17	0.99
	0.01	14.79	13.59	2.93	0.99	76.18	13.2	0.99
	0.05	1.78	18.19	1.75	1.0	53.8	23.66	1.0
	0.1	2.65	0.59	13.48	0.99	3.45	230.4	0.99
	0.3	2.08	0.36	17.67	0.99	3.13	321.7	0.99
	0.5	1.74	0.25	19.61	0.99	1.63	307.9	0.99
Cu–Al–30Ni	0.0	1.28	3.07	5.18	0.99	17.94	28.02	0.99
	0.01	1.61	6.41	3.13	1.0	21.7	36.63	0.99
	0.05	2.24	1.58	8.05	1.0	3.42	116.3	0.99
	0.1	1.91	0.95	16.72	0.99	3.62	220.0	0.99
	0.3	1.91	0.43	14.70	0.99	2.25	354.4	0.99
	0.5	1.59	0.34	18.60	0.99	1.63	308.1	0.99
Cu–Al–45Ni	0.0	2.71	4.44	4.5	0.99	31.39	40.55	0.99
	0.01	2.19	3.55	7.09	0.99	10.66	94.3	0.99
	0.05	1.78	1.85	17.2	0.99	3.0	66.65	0.98
	0.1	2.65	2.23	2.86	1.0	5.13	62.04	0.99
	0.3	2.6	2.86	7.01	1.0	4.78	66.64	0.99
	0.5	1.98	2.55	4.99	0.99	4.77	52.67	0.99

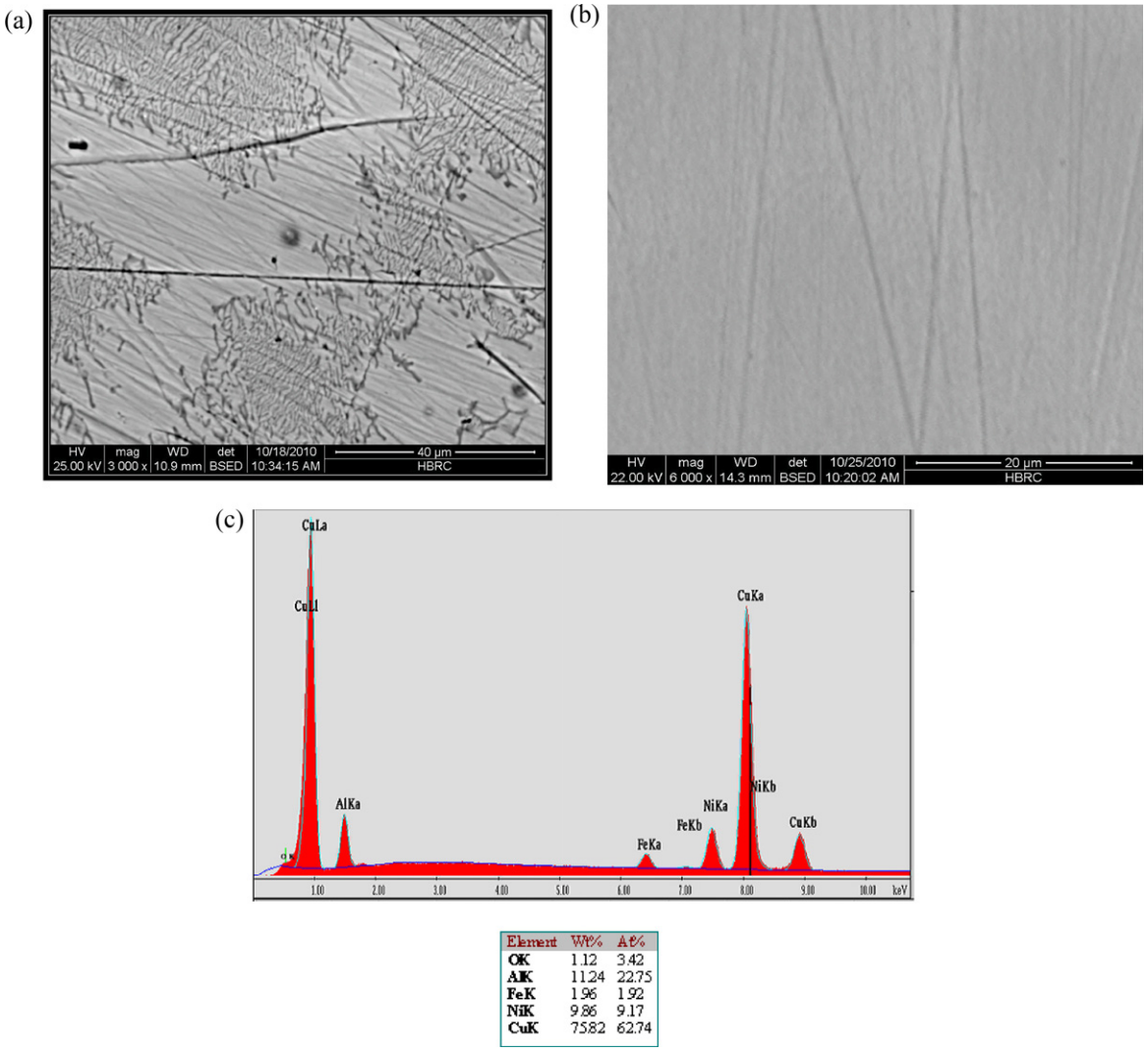

Fig. 7. (a) Scanning electron micrographs of Cu–10Al–10Ni alloys after 3 h immersion in naturally aerated neutral 0.5 M SO_4^{2-} + 0.5 M Cl^- solution at 25 °C. (b) Scanning electron micrographs of Cu–10Al–45Ni alloys after 3 h immersion in naturally aerated neutral 0.5 M SO_4^{2-} + 0.5 M Cl^- solution at 25 °C. (c) EDAX analysis of the Cu–10Al–10Ni alloys after 3 h immersion in naturally aerated neutral 0.5 M SO_4^{2-} + 0.5 M Cl^- solution at 25 °C.

the stability of the barrier film is due to the stable inner adherent layer.

4. Concluding remarks

1. The stability of the Cu–Al–Ni ternary alloys in the stagnant, naturally aerated neutral 0.5 M Na_2SO_4 + 0.5 M NaCl solutions depends on the Ni content.
2. Alloys with Ni content < 30% show relatively higher corrosion rates.
3. The barrier layer that protects the alloy against corrosion is of duplex nature and its breakdown potential decreases with increasing chloride ion concentration.
4. The barrier layer formed on the alloy surface behaves like an ideal capacitor.

References

[1] C.A. Powell, Copper–nickel sheathing and its use for ship hulls and offshore structures, International Journal of Biodeterioration and Biodegradation 321 (1994) 31.
[2] P.K. Chauhan, H.S. Gadiyar, Corrosion Science 25 (1985) 55.
[3] D.A. Jones, Principles and Prevention of Corrosion, second ed., Prentice Hall, Upper Saddle River, NJ, 1996, p. 518.
[4] G. Kear, B.D. Barker, K.R. Stokes, F.C. Walsh, Journal of Applied Electrochemistry 659 (2004) 1235.
[5] J.C. Scully, The Fundamentals of Corrosion, Pergamon Press, Oxford, 1990.
[6] A. Schussler, H.E. Exner, Corrosion Science 34 (1993) 1793.
[7] W.A. Badawy, R.M. El-Sherif, H. Shehata, Journal of Applied Electrochemistry 37 (2007) 1099.
[8] R.F. North, M.J. Pryor, Corrosion Science 10 (1970) 297.
[9] I. Milosev, M.H. Metikos, Electrochimica Acta 42 (1997) 1537.
[10] W.A. Badawy, R.M. El-Sherif, H. Shehata, Electrochimica Acta 54 (2009) 4501.
[11] S.B. Ribotta, L.F. La Morgia, L.M. Gassa, M.E. Folquer, Journal of Electroanalytical Chemistry 624 (2008) 262.
[12] W.A. Badawy, F.M. Al-Kharafi, A.S. El-Azab, Corrosion Science 41 (1999) 709.
[13] W.A. Badawy, M. El-Rabiee, N.H. Hilal, H. Nady, Electrochimica Acta 56 (2010) 913.
[14] A. Bengali, K. Nobe, Journal of the Electrochemical Society 126 (1979) 1116.
[15] S.G. Real, M.R. Barbosa, J.R. Vilche, A.J. Arvia, Journal of the Electrochemical Society 137 (1990) 1696.
[16] E. D'Elia, O.E. Barcia, O.R. Mattos, N. Pebere, B. Tribollet, Journal of the Electrochemical Society 143 (1996) 961.
[17] J.P. Diard, J.M. Le Canut, B. Le Gorrec, C. Montella, Electrochimica Acta 43 (1998) 2469.
[18] K.M. Ismail, A.M. Fathi, W.A. Badawy, Corrosion Science 60 (2004) 795.
[19] F.K. Crundwell, Electrochimica Acta 36 (1991) 2135.
[20] G. Kear, B.D. Barker, K. Stokes, F.C. Walsh, Journal of Applied Electrochemistry 34 (2004) 659.

[21] K. Nobe, G.L. Bauerle, Corrosion 37 (1981) 426.
[22] C. Deslouis, B. Tribollet, G. Mengoli, M.M. Musiani, Journal of Applied Electrochemistry 18 (1988) 374.
[23] G.D. Sulka, P. Jozwik, Intermetallics 19 (2011) 974.
[24] F.M. Al-kharafi, W.A. Badawy, Electrochimica Acta 42 (1997) 579.
[25] J.A. Wharton, R.C. Barik, G. Kear, R.J.K. Wood, K.R. Stokes, F.C. Walsh, Corrosion Science 47 (2005) 3336.
[26] R.G. Blundy, M.J. Pryor, Corrosion Science 12 (1972) 65.
[27] A.-M. Beccaria, J. Crousier, British Corrosion Journal 24 (1989) 49.
[28] M. Urquidi, D.D. Macdonald, Journal of the Electrochemical Society 132 (1985) 555.
[29] M. Metikoš-Huković, R. Babić, I. Škugor, Z. Grubač, Corrosion Science 53 (2011) 347.
[30] J.-D. Kim, S.-I. Pyun, R.A. Oriani, Electrochimica Acta 41 (1996) 57.
[31] K. Hladky, L.M. Calow, J.L. Dawson, British Corrosion Journal 15 (1980) 20.
[32] J. Hitzig, J. Titz, K. Juettner, W.J. Lorenz, E. Schmidt, Electrochimica Acta 29 (1984) 287.
[33] K.M. Ismail, A.A. El-Moneim, W.A. Badawy, Journal of the Electrochemical Society 148 (2001) 81.